

# The sound of Titan

*a role for acoustics in space exploration*

T G Leighton and P R White

This month (July) Cassini, the largest spacecraft ever launched by man, will go into orbit around Saturn.

On Christmas Day 2004 this NASA vehicle will release Huygens, a probe of the European Space Agency, which in early 2005 will undertake a 2.5 hour parachute descent through the atmosphere of Titan, Saturn's largest moon. This probe contains a range of sensors which will communicate data on Titan's atmosphere back to Cassini until Huygens runs out of power. Whilst the primary mission has been directed at investigating Titan's atmosphere, for many the big question is whether or not Titan possesses an equivalent of the features associated with the terrestrial water cycle: seas, lakes, streams, falls, breaking waves, rain etc.

It is possible that Huygens will not answer this question, since its ability to probe the surface is restricted to perhaps three minutes. One item of equipment which might answer this question, whose ruggedness, low power requirements, low mass and small bandwidth make it in many ways an ideal inclusion on a space vehicle, is a microphone. Huygens carries two microphones, primarily to record signals associated with the atmospheric buffeting during the

parachute descent, and to measure the speed of sound in the atmosphere. It is possible that these might record sounds associated with electrical discharge in the atmosphere (as did microphones on the Soviet Union's Venera missions to Venus). However, were the microphones of Huygens to detect the sound of a 'splash-down' end to the parachute descent, the question of Titan's lakes would have been answered. But can we be sure that the sounds we associate with seas and lakes on Earth would find recognisable counterparts on Titan? The object of this article is to explore that question (1). Furthermore, if we have a model for how sound is generated by environmental processes such as falls, wavebreaking and precipitation over a sea, then it is in principle possible to invert the measured sounds to obtain environmental parameters on Titan.

## Cassini, Huygens and Titan

Probably the only place in our Solar System other than Earth which could contain free-flowing surface streams, lakes and seas open to an atmosphere is Titan (*Figure 1*), the largest of Saturn's 20 known moons. At around 1.4 billion

kilometres from the Sun, and 1,221,830 km from Saturn, Titan has a diameter of about 5,150 km, which is around half that of Earth (12,756 km) and slightly larger than that of Mercury. Titan was discovered in 1655 by the Dutch astronomer Christian Huygens. In 1944 another Dutch astronomer, Gerald P Kuiper, confirmed the presence of an atmosphere through spectrographic detection of gaseous methane (CH<sub>4</sub>). The atmosphere generates a reverse greenhouse effect, preventing penetration of solar ultraviolet radiation but allowing infrared to escape Titan.

Currently it is this atmosphere which generates most human interest in Titan. Its outermost fringes extend 600 km into space, ten times further than does Earth's. The reason why Titan (with an escape velocity of 2.7 km/s, compared with 2.4 km/s on Earth's moon, and 11.2 km/s on Earth) has a dense atmosphere (the only moon in the Solar System to do so), whereas Mercury (with an escape velocity of 4.5 km/s) does not, is because Titan's low surface temperature (-180 °C, 93 K) keeps atmospheric molecular velocities below escape velocity. With an atmospheric pressure at the surface which is one and a half times that of Earth, the major gas component is nitrogen (90%). It was probably formed by the solar ultraviolet breakdown of ammonia (NH<sub>3</sub>) deposited from comets, producing N<sub>2</sub> and hydrogen (which is sufficiently light to escape Titan's gravity). Other components include argon (10%), hydrogen cyanide (HCN), ethane, methane, propane (C<sub>3</sub>H<sub>8</sub>) (2).

This rich chemistry results from solar radiation and the passage of Titan through the vast fields of charged particles which are trapped by Saturn's magnetic field. There are methane clouds at an altitude of 25 km (although only 1% of the surface is covered by cloud, compared with 50% on Earth). However the atmosphere is very thick and hazy owing to suspended aerosols and condensates of hydrocarbons, forming a smog which is much thicker than any over cities on Earth. Although the temperature would predispose against the formation of life at the surface of Titan

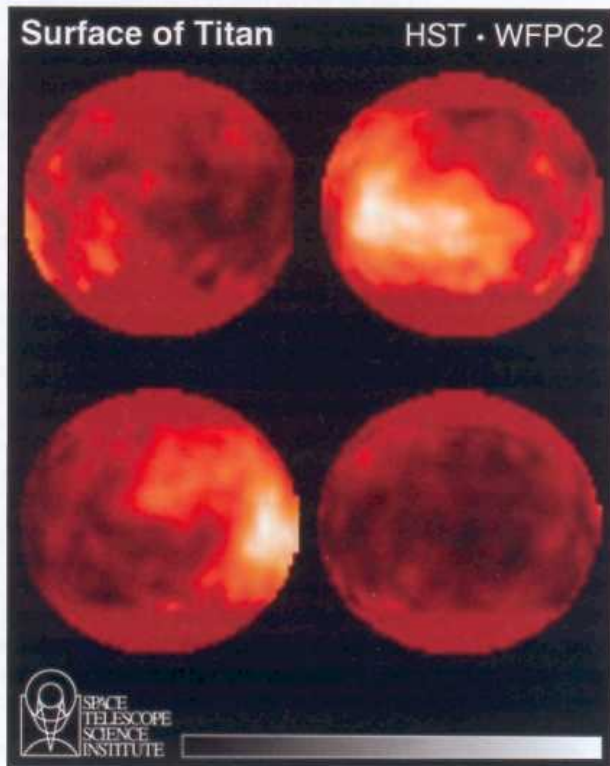


**Figure 1:** four global projections of Titan, separated in longitude by 90 degrees, taken by the Hubble Space Telescope's WideField/Planetary Camera 2 at near-infrared wavelengths (between 0.85 and 1.05 microns). Upper left: hemisphere facing Saturn. Upper right: leading hemisphere (brightest region). Lower left: the hemisphere which never faces Saturn. Lower right: trailing hemisphere. These assignments assume that the rotation is synchronous. The single prominent bright area is a surface feature 2,500 miles across, about the size of the continent of Australia, and may be a continent. (Image credit: P. H. Smith and M. Lemmon of the UA Lunar and Planetary Laboratory, and NASA)



**Figure 2:** the launch of *Cassini-Huygens* on 15 October 1997. (Image credit: NASA/JPL/Caltech)

(noting that in principle locally higher temperatures may be generated on moons through radiation and geothermal processes, meteorite impacts, lightning, seismic activity etc.), the potential for these chemicals to provide a pre-biotic environment similar to that of Earth during the early stages of the evolution of life has stimulated interest in Titan, and even prompted speculation that it might support life when our Sun becomes a red giant.

At \$3.4 billion the Cassini-Huygens mission is one of the most expensive ever launched, a collaboration between seventeen countries and three space agencies (NASA, the European Space Agency and the Italian Space Agency). Probably the most complex space mission launched, its start was controversial: the 5650 kg Cassini-Huygens bus-sized craft is not only the largest launched, but also carries the greatest mass of plutonium 238 (32.5 kg) ever put into space. This raised fears in some quarters of a possible disaster at its launch on October 15 1997 using a massive Titan IV-B/Centaur launch vehicle from Florida's Cape Canaveral Air Station (*Figure 2*), and the later Earth fly-by in August 1999 which was designed to exploit Earth's gravity in a 'sling-shot' manoeuvre.

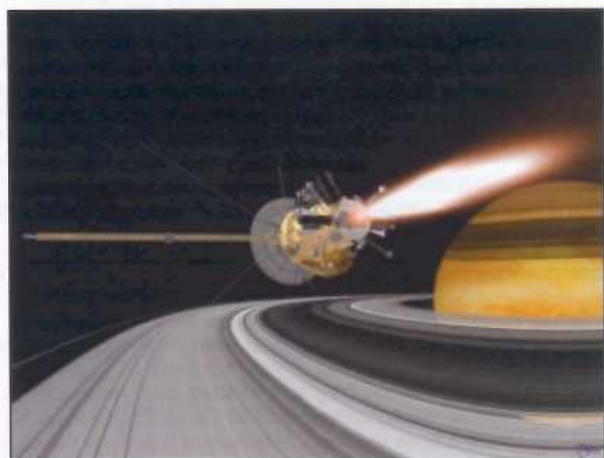


**Figure 3:** this is a computer-rendered image of *Cassini-Huygens* during the Saturn Orbit Insertion (SOI) manoeuvre, just after the main engine has begun firing. The spacecraft is moving out of the plane of the page and to the right (firing to reduce its spacecraft velocity with respect to Saturn) and has just crossed the ring plane. The 96 minute SOI manoeuvre will allow *Cassini-Huygens* to be captured by Saturn's gravity into a five-month orbit. (Image credit: NASA/JPL/Caltech)

Following a flyby of Phoebe (the outermost moon orbiting Saturn) at an altitude of 2000 km on 11 June 2004, NASA's Cassini on 1 July 2004 crosses Saturn's ring plane during the spacecraft's critical Saturn Orbit Insertion manoeuvre (*Figure 3*) It will fire its engine for 96 minutes to become the first man-made object to enter orbit around Saturn, passing 15000 km above the rings and within 20000 km of its outer atmosphere. During its 4-year orbital study of the Saturn system, Cassini will pass Titan several times, making radar maps of its surface.

Piggybacking on Cassini is the European Space Agency's Huygens probe, which is scheduled to be the first man-made spacecraft ever to land on the moon of another planet. After a seven-year journey strapped to its side, Huygens will separate from Cassini at a relative speed of 30 cm/s on 25 December 2004, then coast for 20 days on its way to Titan, and finally enter the moon's atmosphere on 14 January 2005. This is seven weeks later than originally planned, in order to minimise the effect of a telecommunications problem, which would have resulted in loss of data transmitted to Cassini from Huygens through failure to compensate for the Doppler shift on the radio signals between the two. In the original flight plan, Cassini would be rapidly approaching Titan during Huygens' 2.5 hour parachute descent through the thick atmosphere. It will now fly over Titan's clouds at an altitude of 65000 km, more than fifty times higher than originally planned (hence the discrepancy between the eventual orbit and those illustrated in *Figure 4* and *Figure 5*).



**Figure 4:** an artist's impression of Titan's surface, with Saturn dimly visible in the background through Titan's thick atmosphere. The *Cassini* spacecraft flies over the surface with its High Gain Antenna pointed at the *Huygens* probe as it nears the end of its parachute descent. Thin methane clouds dot the horizon, and a narrow methane spring or 'methanefall' flows from the cliff at left and produces considerable vapour. Smooth ice features rise out of the methane/ethane lake, and crater walls can be seen far in the distance. (Illustration by David Seal, Image credit: NASA/JPL/Caltech)

Huygens will now need to be pre-heated to improve tuning of the transmitted signal. Cassini's arrival date at Saturn is unaltered (1 July 2004), and the flybys of Titan will occur on 26 October and 13 December 2004. From February 2005 Cassini will continue on its four year primary mission of studying Saturn's rings, moon and magnetic field.

Huygens' primary mission is to analyse the atmosphere during this descent. Examination of Titan's surface is limited by the lifetime of the five onboard batteries, which are capable of generating 1800 Watt-hours of electricity. These will constrain the Huygens mission to just 153 minutes, corresponding to a maximum descent time of 2.5 hours plus at least three additional minutes (and possibly an extra half

*continued on page 18*

# The sound of Titan

a role for acoustics in space exploration

continued from page 15

hour) on Titan's surface. It is hoped that Huygens will be able to record images from the surface of Titan. The dense smog proved to be impenetrable at the visible wavelengths utilised by the cameras aboard the Pioneer and Voyager spacecraft that flew past Saturn in the late 1970s and early 1980s. Earth-based radar, however, and near-infrared wavelengths from the Hubble telescope (*Figure 1*) have indicated the possible existence on Titan of lakes and seas consisting of hydrocarbons, mainly ethane  $C_2H_6$ . There are probably mountains which include water ice.

The surface conditions on Titan are close to triple point of methane/ethane, and therefore it is possible that methane/ethane may play a similar role on Titan as does water on Earth, with methane/ethane seas, methane/ethane ice and methane/ethane vapour. Hence on a Titan beach, should one exist, the sea may be fed by streams, falls, and rain consisting primarily of methane (which, on Earth, is the main component of the domestic heating fuel 'natural gas'). Although tidal forces are 400 times greater than on Earth, like most of Saturn's moons Titan is tidally locked, keeping the same face oriented towards the planet during its 16-day synchronously rotating orbit. As a result, massive tides will not be seen on these possible seas. However Titan's orbit is elliptical, and as the distance to Saturn (and its moons) changes over this 16-day month a tide of about 3m would not be unexpected, nor would gravitationally generated winds of a few metres per second. Neither, therefore, would sea waves be surprising if such a sea exists, and indeed these might be detected by accelerometers on Hygens. Given appropriate parameters, it should be possible to predict the sound generated on Titan by such natural phenomena, and this will now be done for the underwater sound of falls (*Figure 4*) (with associated recordings for these, 'splash-down' and breaking waves, available via <http://www.isvr.soton.ac.uk/fdag/uaua.htm>). The necessary physical parameters are summarised in *Table 1*, the values for Titan being estimates.



**Figure 5:** an alternative rendering of the Huygens descent, showing clouds at 20 km altitude. The descent will occur during daylight to provide the best illumination conditions for imaging the clouds and surface. (Illustration by Craig Attebery, Image credit: NASA/JPL/Caltech)

## Method

### Bubble dynamics

This paper will illustrate the possibilities of acoustic inversion by predicting the pressure signal which an underwater microphone (a hydrophone) might measure close to Titan's equivalent of a waterfall. This is first-order estimation, and based on two key simplifications. The first is that the pressure signature above a certain frequency is dominated by bubble sources of sound, whilst below that frequency non-bubble sources (e.g. hydrodynamic) are mainly responsible. The second arises because the technique requires input of a bubble size distribution for Titan. Until a better estimate for use with the method of this paper is found, this first calculation will assume that bubbles generating audio-frequency sound will follow the distribution found in a terrestrial waterfall. This is not an unreasonable first guess given the dynamics of gas entrainment by waterfalls and the fluid properties (*Table 1*). The issue of wave-breaking in the large waves that might result from Titan's low gravity is more complicated.

When, in response to an impulse excitation, a bubble pulsates at low amplitude about an equilibrium radius ( $R_0$ ), it resembles a damped harmonic oscillator: the stiffness is invested primarily in the gas, and the inertia arises mainly through the surrounding liquid, which must move if the bubble wall is to oscillate (3). Spherical pulsations only will be considered here, because they dominate the far-field radiation. Damping can arise through many sources, but for

		EARTH	TITAN
<b>LIQUID:</b>		<b>Water</b>	<b>Mainly ethane</b>
Surface tension ( $\sigma$ )	$N m^{-1}$	0.075	$0.031 \pm 10\%$
Vapour pressure ( $p_v$ )	Pa	3500	$2.2 \pm 10\%$
Dynamic viscosity ( $\eta$ )	$Ns m^{-2}$	$1.433 \times 10^{-3}$	$1.12 \times 10^{-3} \pm 10\%$
Mass density ( $\rho$ )	$kg m^{-3}$	999.93	$648.4 \pm 5\%$
Sound speed ( $c$ )	$m s^{-1}$	1434.4	$1982 \pm 2\%$
<b>GAS</b>		<b>Air</b>	<b>Mainly nitrogen</b>
Thermal conductivity ( $K_g$ )	$W m^{-1} K^{-1}$	0.02598	$0.0088 \pm 5\%$
Molar heat capacity ( $C_{p,m}$ )	$J mol^{-1} K^{-1}$	28.96	$26.9 \pm 3\%$
Mass density ( $\rho_l$ )	$kg m^{-3}$	1.293	6.131
Molecular diameter ( $l_g$ )	m	$3.15 \times 10^{-10}$	$3.15 \times 10^{-10}$
Molecular mass ( $m_g$ )	kg	$4.99 \times 10^{-26}$	$4.99 \times 10^{-26}$
Specific heat at constant pressure ( $C_p$ )	$J kg^{-1} K^{-1}$	$1.0414 \times 10^3$	$1.03 \times 10^3 \pm 7\%$
Specific heat at constant volume ( $C_v$ )	$J kg^{-1} K^{-1}$	$0.7429 \times 10^3$	$0.76 \times 10^3 \pm 7\%$
Ratio of specific heat at constant pressure to that at constant volume ( $\gamma = C_p / C_v$ )		1.402	$1.45 \pm 10\%$
Speed of sound ( $c_g$ )	$m s^{-1}$	334	192.5
<b>Local parameters</b>			
Temperature	K	283	93
Atmospheric pressure	Pa	$10^5$	$1.5 \times 10^5$
Acceleration due to gravity ( $g$ )	$m s^{-2}$	9.81	1.35
<b>Fundamental parameters</b>			
Boltzmann's constant ( $k_B$ )	$J K^{-1}$	$1.38 \times 10^{-23}$	$1.38 \times 10^{-23}$
Avogadro's number ( $N_A$ )		$6.023 \times 10^{23}$	$6.023 \times 10^{23}$

**Left:** *Table 1* properties relevant to the generation of underwater sound by bubbles at surface of Earth and Titan. The sources of the Titan parameters are very numerous, from formal to informal, and at times contradictory. Hence they are not cited, and researchers wishing to undertake similar calculations are encouraged to carry out independent searches for these parameters. Because no value of any parameter listed in the table is derived from the value listed for another, certain internal consistency checks (e.g.  $C_{p,m} = N_A m_g C_p$  and  $\gamma = C_p / C_v$ ) will not behave as expected. The decision was made to use what were judged to be the best values available, rather than force internal consistency. Although values of gas thermal diffusivity  $D_g$  at atmospheric pressure are available in the literature, for the calculations here  $D_g$  was calculated from  $K_g$  so that any dependence of  $D_g$  on bubble size (through surface tension) could be incorporated. (TGL is grateful to P R Birkin for checking the estimates he made in this table)

most gas bubbles in liquids the primary ones are associated with viscous losses in the liquid as the wall moves, with radiation losses as acoustic energy propagates away from the bubble, and with thermal losses as the gas is compressed and rarefied during the pulsation. Most bubbles on Earth are lightly damped, and on entrainment are not at equilibrium (Figure 6) such that their subsequent wall motions, and acoustic pressure emissions, resemble exponentially decaying sinusoids at the bubble natural frequency  $\nu_0$  (Figure 7). In 1933, Minnaert (4) hypothesised that this might be the source of 'the murmur of the brook, the roar of the cataract, or the humming of the sea'; and in 1987 a bubble population in the natural world (under a waterfall) was for the first time estimated using such passive entrainment emissions (5). In 1991 this was done for breaking waves, where the entrainment rates were far greater (6).

The key characteristics of such low-amplitude natural oscillations (quality factors and natural frequencies) can readily be calculated for air bubbles in water on Earth (7, 8, 9). The undamped natural frequency can of course be estimated from the square root of the ratio of the stiffness of the bubble gas to the inertia of the associated liquid. The stiffness of the gas is itself dependent on the relationship between the pressure  $p$  and the volume  $V$  in the gas. A useful engineering approximation is to characterise this by

*continued on page 20*

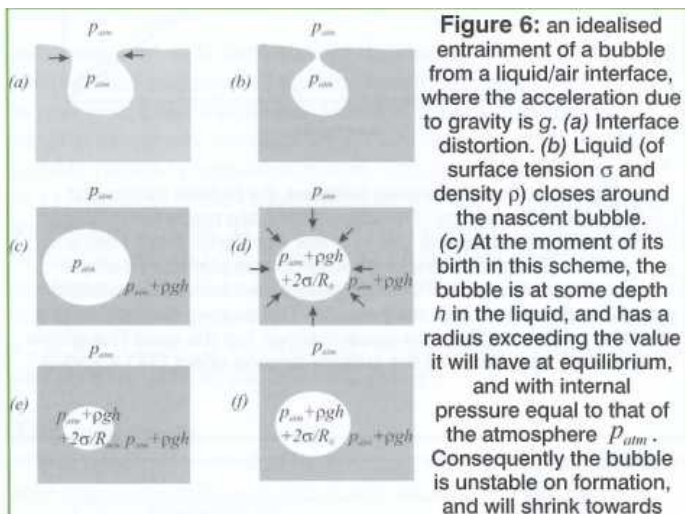


**Figure 6:** an idealised entrainment of a bubble from a liquid/air interface, where the acceleration due to gravity is  $g$ . (a) Interface distortion. (b) Liquid (of surface tension  $\sigma$  and density  $\rho$ ) closes around the nascent bubble. (c) At the moment of its birth in this scheme, the bubble is at some depth  $h$  in the liquid, and has a radius exceeding the value it will have at equilibrium, and with internal pressure equal to that of the atmosphere  $P_{atm}$ . Consequently the bubble is unstable on formation, and will shrink towards

equilibrium (where in this approximation internal pressure will match that of the surrounding liquid,  $p_{atm} + \rho gh$ , plus the Laplace pressure  $2\sigma / R$ , commensurate to its size [3§2.1.1]). (d) Therefore the bubble contracts, passes through equilibrium size because of the inertia of the surrounding liquid, until (e) the work done by the compressed gas halts the wall motion at some minimum bubble radius  $R_{min}$ , and starts the rebound. The bubble undergoes pulsations, the amplitude of which decay through radiation, viscous, thermal and any other losses, until (f) it is stationary at equilibrium size

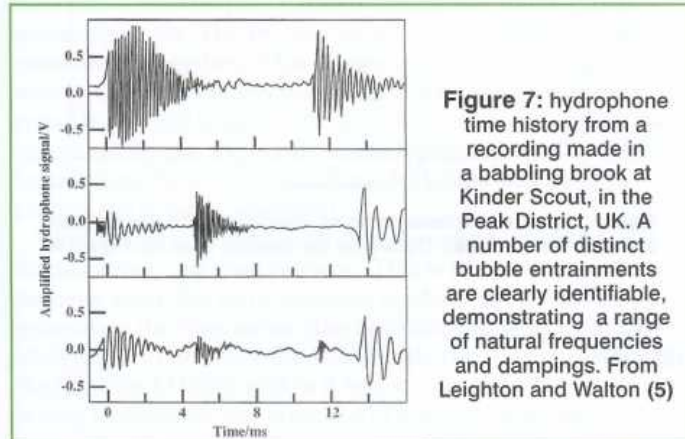


**Figure 7:** hydrophone time history from a recording made in a babbling brook at Kinder Scout, in the Peak District, UK. A number of distinct bubble entrainments are clearly identifiable, demonstrating a range of natural frequencies and dampings. From Leighton and Walton (5)

# The sound of Titan

*a role for acoustics in space exploration*  
continued from page 19

a polytropic index,  $k$ , such that for a perfect gas  $pV^\kappa = \text{constant}$ , where  $\kappa$  can take values between  $\gamma$  (the ratio of the specific heat of the gas at constant pressure,  $C_p$ , to that at constant volume,  $C_v$ ) and unity, depending on whether the pulsations are adiabatic, isothermal, or of an intermediate nature (10). Of course since  $pdV$  is a perfect differential, the use of a polytropic index that is constant during the

oscillatory cycle of a given bubble can never describe net thermal losses from the bubble (11). In this limit, that is done by characterising a dimensionless damping coefficient  $\delta_{tot}$  for the bubble undergoing natural pulsations, such that  $\delta_{tot}$  is the reciprocal of the quality factor of the bubble. In turn,  $\delta_{tot}$  is a simple summation of the dimensionless damping coefficients calculated for viscous losses ( $\delta_{vis}$ ), acoustic radiation losses ( $\delta_{rad}$ ), and net thermal losses ( $\delta_{th}$ ).

Expressions for these have remained largely unchanged since the 1950's, except for a suggested correction [3§3.4.1b(iv)] to the use in  $\delta_{th}$  of a constant thermal diffusivity for the gas ( $D_g$ ). Strictly, this depends on the gas

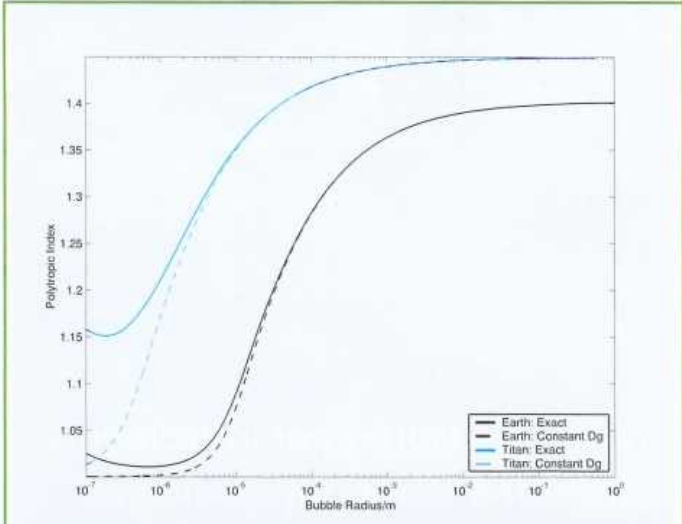


**Figure 8:** calculated values of the polytropic index for gas bubbles pulsating at their natural frequencies. The calculations are made for bubbles containing atmospheric gas in water (for Earth, black lines) and ethane (Titan, blue lines) with appropriate planetary surface conditions (Table 1). In each case, two curves are plotted (solid and dashed). The dashed lines assume a constant value for  $D_g$  in the usual manner, but the solid lines allow  $D_g$  to vary as a result of the surface tension effect [3§3.4.2b(iv)]. The calculations for Titan are based on the estimated values in Table 1. Whilst the trends seem realistic, the offset between the two curves falls within the uncertainty of the values in Table 1

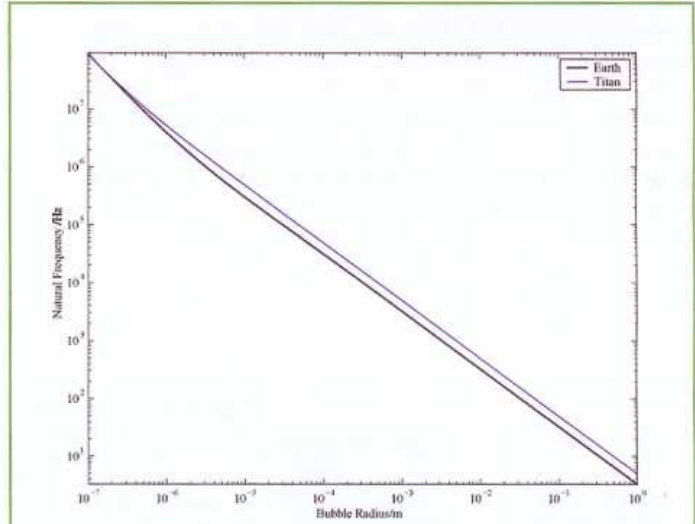


**Figure 9:** the relationship between the bubble radius and the natural frequency. The calculations are made for bubbles containing atmospheric gas in water (for Earth, black line) and ethane (Titan, blue line) with appropriate planetary surface conditions (Table 1). For each planet, two curves are plotted (solid and dashed), but they overlap. The dashed line assumes a constant value for  $D_g$  in the usual manner, but the solid line allows  $D_g$  to vary as a result of the surface tension effect [3§3.4.2b(iv)]

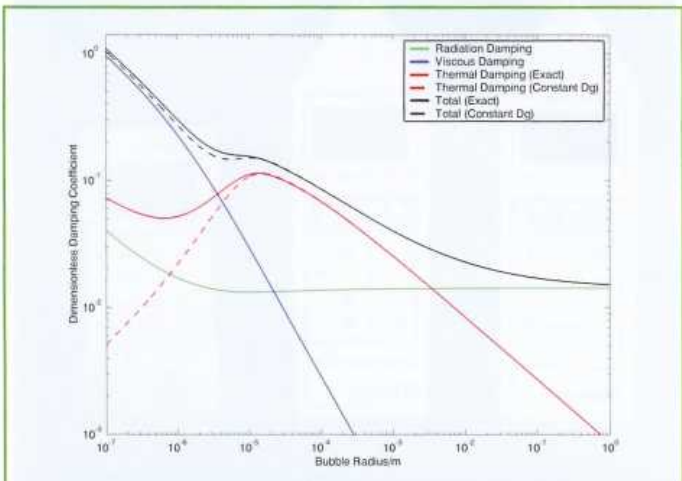


**Figure 10:** damping coefficients for air bubbles in water at standard conditions for the surface of the Earth. The thermal ( $\delta_{th}$ , red), viscous ( $\delta_{vis}$ , blue), and radiation ( $\delta_{rad}$ , green) damping coefficients are plotted, as is their sum, the total dimensionless damping coefficient ( $\delta_{tot}$ , black). For the thermal and total coefficients, two curves are plotted. In each case, the dashed line assumes a constant value for  $D_g$  in the usual manner, but the solid line allows  $D_g$  to vary as a result of the surface tension effect [3§3.4.2b(iv)]. These calculations are based on the estimates of Table 1

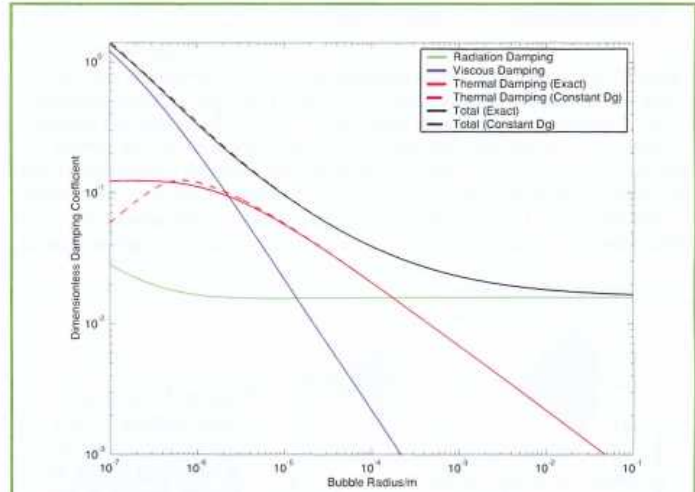


**Figure 11:** dimensionless damping coefficients for gas bubbles at the surface of Titan. Otherwise the caption is as for Figure 10

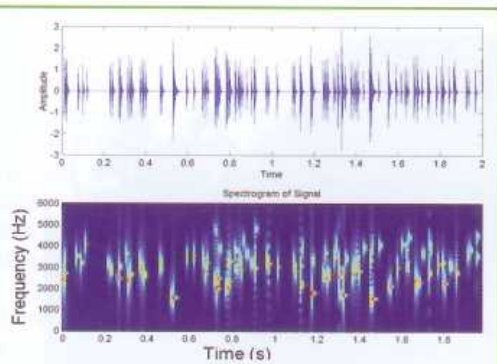


**Figure 12:** the upper plot shows an artificially constructed hydrophone signal when fifty bubbles per second are introduced without noise. The spectrogram of this signal is shown in the lower plot, which displays high acoustic energy as 'hot' colours, distributed across frequency bands as indicated in the vertical axis, at times as marked on the horizontal axis. In the spectrogram it is easy to identify the frequency of the individual bubbles and their amplitude. This signal can be heard via <http://www.isvr.soton.ac.uk/fdag/uaua.htm>, where it is very easy to hear the individual bubble signals. However it does not sound like realistic rain or a babbling brook

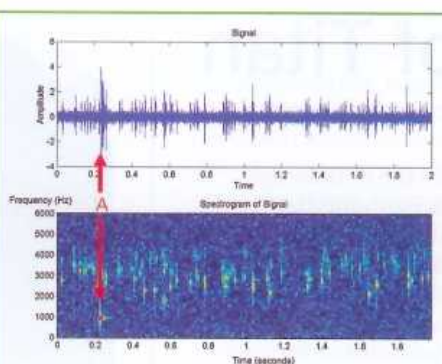


**Figure 13:** a two-second hydrophone time history (upper plot) and the corresponding spectrogram (lower plot) are constructed with the same underlying statistics for the bubble size distribution as in Figure 12, and with the same rate of bubble generation (50 per second), but with added random Gaussian noise at a similar level to that which might be found at some natural sites on Earth. This signal can be heard via <http://www.isvr.soton.ac.uk/fdag/uaua.htm>, where it sounds a little more like rain or a babbling brook than do the data of Figure 12. You should be able to hear a high amplitude, low-frequency signal from a large bubble near the beginning of the recording (labelled A)

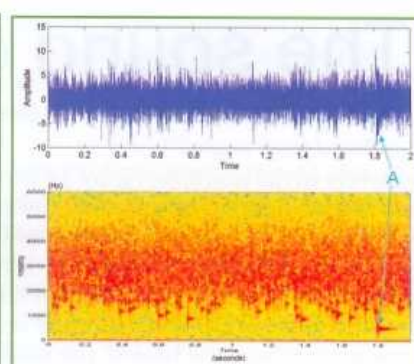


**Figure 14:** a two-second hydrophone time history (upper plot) and the corresponding spectrogram (lower plot) are constructed with the same underlying statistics for the bubble size distribution and statistics for added noise as in Figure 13, but the bubble generation rate has increased to 2500 per second. This signal can be heard via <http://www.isvr.soton.ac.uk/fdag/uaua.htm>, where it sounds a lot more like rain or a babbling brook than do the data of Figures 12 or 13. You should be able to hear a high amplitude, low-frequency signal from a large bubble near the end of the recording (labelled A)

pressure, and so in turn should depend on the bubble radius through the influence of surface tension (Figure 6(d)-(f)). In practice, in air bubbles in water on Earth, the effect for natural frequency oscillations is only significant when the bubble radius is sub-micrometre. This is evident in Figures 8 to 11, which plot the polytropic index (Figure 8) and natural frequencies (Figure 9), as a function of the equilibrium radius of the bubble; and the various dimensionless damping coefficients for natural frequency oscillations on Earth (Figure 10) and Titan (Figure 11). Note that for macroscopic bubbles  $v_0 \propto R_0^{-1}$  (Figure 9). Having determined these quantities, they can now be used in the acoustic model.

### The inversion

The required inversion here entails estimating the bubble size distribution from the acoustic emissions (10). Since in nature the result is normally not amenable to independent verification (11), the efficacy of the technique will first be illustrated using simulated acoustic data. The model (see previous section) for the sound field that a single bubble generates on entrainment is programmed into a PC, and the PC then chooses the statistics of the bubble size distribution from which it wishes to predict the acoustic emission. Appropriate randomisation is given to the positioning of the bubble with respect to the hydrophone, the depth of entrainment etc. The PC then generates an artificial acoustic pressure time history. This is then inverted by a program which is ignorant of any information regarding the bubble population used to generate that time series, other than the nature of the gas, the nature of the liquid, the depth of the hydrophone, and the physical model which was used to predict the acoustic emission.

This programme then estimates the original bubble size distribution using the inversion. This is of course a trivial process, since the same physical model is used both for generating the time series (the 'for problem') and for inverting it to estimate the bubble size distribution, although the addition of noise makes it less so. However this exercise is only to illustrate the potential of the technique before it is

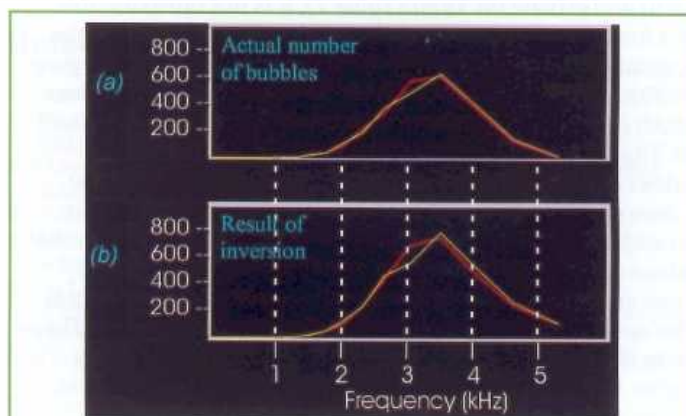


**Figure 15:** inversion of the data of Figure 14 produces the bubble population given in (b), the lower plot (the red curve corresponding to the bubbles which are generated in the first second of the hydrophone trace, and the yellow curve to those generated between 1 and 2 seconds). The number of bubbles counted is plotted as a function of their natural frequencies, which in turn can be readily related to bubble size through Figure 9. Having in the lower plot estimated the bubble population the computer used to generate the time series, this can be compared with the upper plot (a) to see the actual bubble population that was used by the PC in generating the acoustic time history of Figure 14. The degree of agreement illustrates the degree to which the inversion has been successful. The centre frequencies (in Hz) for the bins above 1000 Hz are: 1000, 1149, 1320, 1516, 1741, 2000, 2297, 2639, 3031, 3482, 4000, 4595, 5278

applied to real acoustic time series, where the true 'answer' (the bubble size distribution) will not be known. Figures 12 to 14 show three two-second predictions of the acoustic emission for the same bubble size distribution, but with increasing levels of complexity in the sound field as noise is added and the entrainment rate increased. Figure 15 shows that the bubble size distribution estimated by the inversion of the data of Figure 14 resembles the actual bubble size distribution used to predict the acoustic time series.

Having illustrated the efficacy of the inversion in this

*continued on page 22*

# The sound of Titan

*a role for acoustics in space exploration*

*continued from page 21*

relatively trivial example, *Figure 16* shows the bubble size distribution inferred by inverting the acoustic emission generated in a waterfall to provide an estimate of the population of 'ringing' bubbles (as distinct from the full bubble population which optical techniques or active sonar might measure (11)). The data were recorded by TGL around three metres from the base of the small waterfall at Sadler's Mill, Romsey, Hampshire (*Figure 17*). "This beauty spot is known as 'salmon leap', recollecting the dull Autumn days when the fish leapt out of the water as they struggled to return upstream to their breeding grounds" (12). From the statistics of this bubble size distribution it is possible to reconstruct a time series, as described above, randomly selecting bubbles for placement in that time series based upon the statistics of *Figure 16*: whilst the exact form of the reconstructed time series or time-frequency representation will not of course be identical to the original, the two spectra should be very similar. This procedure will now be conducted.

## Predicting the sound of falls on Earth and Titan

Given the similarity in fluid properties between water on Earth and ethane on Titan (*Table 1*), it is not unreasonable as a first approximation to assume that the statistics of the populations generated by falls in the audio frequency regime on Titan are similar to terrestrial ones. Assuming a receiver depth of 10 cm, and exploiting the relationships determined for Titan between the bubble radius and the polytropic index (*Figure 8, blue curve*) and natural frequency (*Figure 9, blue curve*), it is possible to construct hydrophone time series based on the statistics of *Figure 16*, obtained from the Salmon Leap at Sadler's Mill (*Figure 17*). *Figure 18* shows three spectrograms, taken from time series of 10 s duration. The upper plot is from the signal recorded at the site of *Figure 17*. In this, that component of the signal with a frequency higher than 1 kHz was designated as being due to bubbles (in addition a low-pass filter set to 17.5 kHz was applied, since the Salmon Leap data was recorded with a sampling

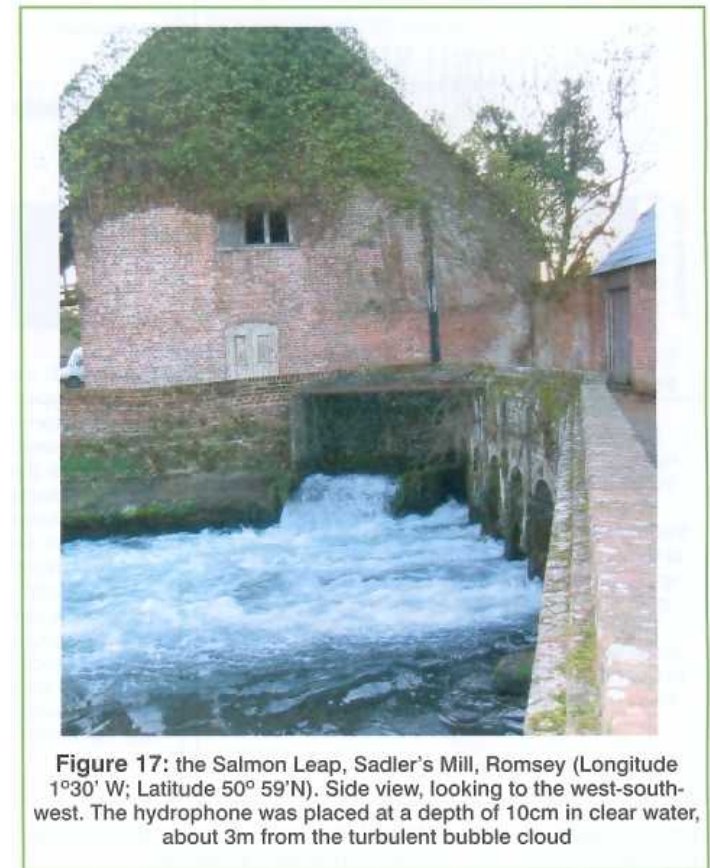


**Figure 17:** the Salmon Leap, Sadler's Mill, Romsey (Longitude 1°30' W; Latitude 50° 59'N). Side view, looking to the west-south-west. The hydrophone was placed at a depth of 10cm in clear water, about 3m from the turbulent bubble cloud

frequency of 44.1 kHz). It was this component which was then used to infer the population of *Figure 16*.

The middle plot of *Figure 18* shows a spectrogram constructed using the statistics of the population of *Figure 16*, for Earth. It is not of course intended to mimic the upper plot, for two reasons. First, it is constructed using only that portion of the data in the Salmon Leap recording which was identified as being generated by bubbles (and hence low frequency noise, hydrodynamic fluctuations etc. which are present in the upper plot are not included in the middle plot). Second, the exact time and natural frequency of the entrainment of a given bubble is determined at random, constrained to the statistics of the population of *Figure 16*. The same process is repeated in the lower plot for the conditions on Titan. There is clearly more energy at the higher frequencies, a fact confirmed by examination of the power spectra (taken over 10 s of data) in *Figure 19*. Whilst the reconstructed Earth waterfall (green line) closely resembles the original Salmon Leap spectrum (blue line), the slope of the Titan spectrum (red line) is more shallow, and the overall level increased by up to -10 dB in the audio range. A quick check in the tendency to generate higher frequencies is found through inputting the data of *Table 1* into Minnaert's theory (4, 10) to reduce Earth's  $\nu_0 R_0 \approx 3.26 \text{ Hz.m}$  relationship for audio-frequency air bubbles in water under surface atmospheric pressure, to  $\nu_0 R_0 \approx 5.05 \text{ Hz.m}$  for Titan. Hence the change in spectral slope seems reasonable. The -10 dB increase in levels for the population of *Figure 16* is less certain at this stage, the extrapolation from excitation (*Figure 6*) on Earth to that on Titan involving significant speculation (10).

## Discussion

The same procedure has been applied to estimate the underwater sound of breaking waves, and solid body impacts ( splash downs) on Titan. Sound files are available via <http://www.isvr.soton.ac.uk/fdag/uaua.htm>

Acoustic techniques, particularly passive ones, might be

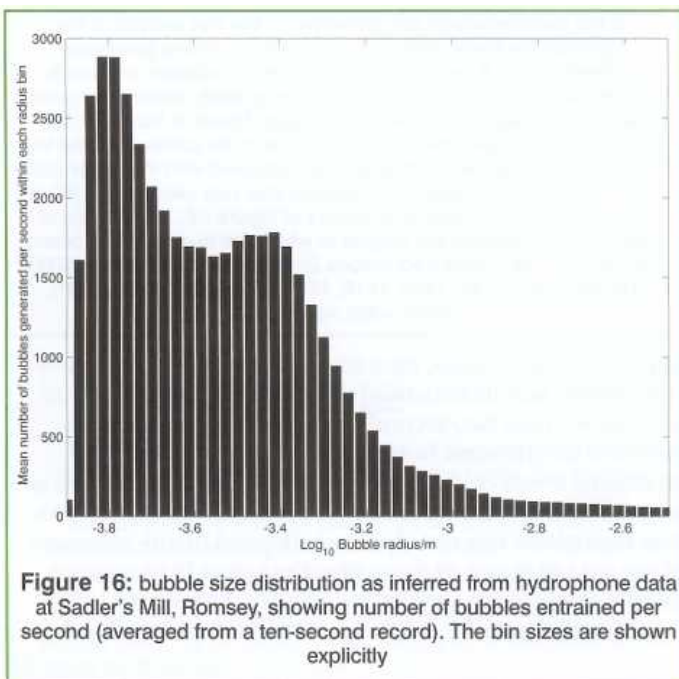


**Figure 16:** bubble size distribution as inferred from hydrophone data at Sadler's Mill, Romsey, showing number of bubbles entrained per second (averaged from a ten-second record). The bin sizes are shown explicitly

applied cheaply to investigate a range of effects on planets and moons, including wind, storms and lightning, turbulence and hydrodynamic effects, volcanic activity, seismology and geophysics, gravitational forces (indirectly), boiling and precipitation, rockfalls etc. Passive sonar can indeed use the reverberation from natural sources, (particularly meteorite impacts, volcanic events, or ice cracking which can give rise to transient signals) to provide a low-cost quasi-active bistatic sonar.

Europa (13) may support a water ocean beneath a covering of ice. Estimates of the ocean depth and ice thickness give values far greater than those found on Earth, respectively ranging up to 100 km and 2-20 km. While this environment presents considerable challenges for placing a vehicle in these ocean depths, sound from

those depths will propagate up to the surface. The ambient noise in that ocean may contain contributions from such environmentally significant features as ice cracking, hydrothermal vents, meteorite strikes, seismic activity etc. Off-world environments (real or laboratory) would also give the opportunity to test exotic acoustic effects. For example, it has been proposed (14) that peaks in ocean ambient noise arise through a resonance-like interaction between zero- and high-order modes of oscillation of the bubble wall, and the bubble radii (and hence frequencies) at which these occur depend on environmental parameters such as atmospheric pressure [383.6, 14].

Is there any purpose to such extraterrestrial speculation? The passive acoustic techniques described above exploit a small amount of processing, power requirements and rugged hardware, in comparison with most sensors on space probes. The signal bandwidth is very much less than that required for images, facilitating rapid transmission to an orbiter and thence to Earth. These features make acoustic sensors particularly suitable for deployment from a space probe, where of course energy, weight and communication restrictions are critical. Given that passive acoustic emissions have been used to provide such a range of environmental information on Earth (15), it is worth considering how far acoustic information may be inverted to reveal the environmental information about the craft, space, and particularly the bodies on which they land.

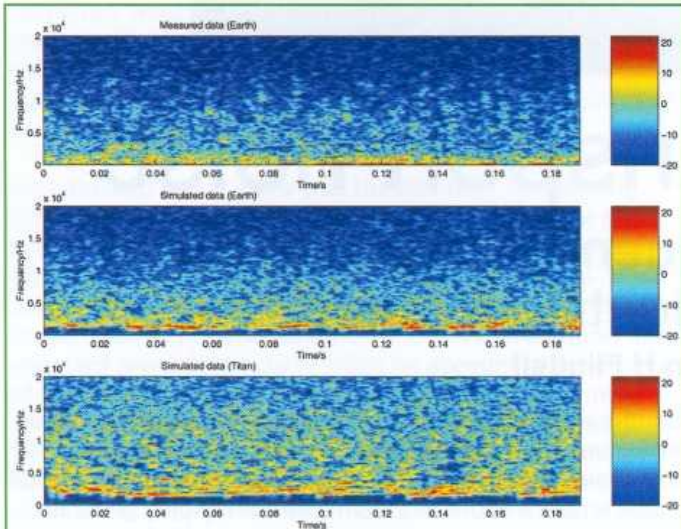


**Figure 18:** spectrogram of a sample of the time series hydrophone signals. Upper plot: measured signal on Earth at site of Figure 17. Middle plot: spectrogram reconstructed for Earth using the population statistics of Figure 16. Lower plot: spectrogram reconstructed for Titan using the population statistics of Figure 16. These recordings can be heard via <http://www.isvr.soton.ac.uk/fdag/uaua.htm>

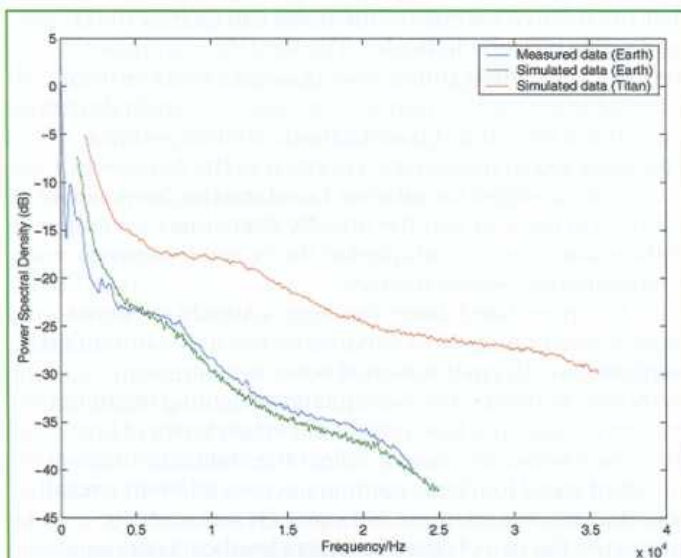


**Figure 19:** power spectral densities of 10s signals for: the signal recorded at site of Figure 17, from which those components due to bubbles were identified and used to infer the population of Figure 16 (blue line); the signal containing only bubble-generated components, for Earth, predicted by applying the model of (10) to the population of Figure 16 (green line); the signal containing only bubble-generated components, for Titan, predicted by applying the model of (10) to the population of Figure 16 (red line)

## References

- 1 T G Leighton, The Tyndall Medal paper: From sea to surgeries, from babbling brooks to baby scans: bubble acoustics at ISVR *Proceedings of the Institute of Acoustics*, **26**, Part 1, 357-381 (2004)
- 2 R Lorenz and J Mitton, *Lifting Titan's veil* (Cambridge U Press, 2002)
- 3 T G Leighton, *The Acoustic Bubble* (Academic Press, 1994)
- 4 M Minnaert, On musical air-bubbles and sounds of running water, *Phil Mag* **16**: 235-248 (1933)
- 5 T G Leighton and A J Walton, An experimental study of the sound emitted from gas bubbles in a liquid *Eur J Phys* **8**: 98-104 (1987)
- 6 M R Loewen and W K Melville, A model for the sound generated by breaking waves *JAoust Soc Am* **90**: 2075-2080 (1991)
- 7 H Pfiem, *Zur thermischen dämpfung in kugelsymmetrisch schwingenden gasblasen* *Akust Zh* **5**: 202-207 (1940)
- 8 Z Saneyoshi, *Electro-technical Journal* (Japan) **5**: 49 (1941)
- 9 C Jr Devin, Survey of thermal, radiation, and viscous damping of pulsating air bubbles in water *JAoust Soc Am* **31**: 1654-1667 (1959)
- 10 T G Leighton, From babbling brooks to baby scans, from seas to surgeries: The pressure fields produced by non-interacting spherical bubbles at low and medium amplitudes of pulsation, *International Journal of Modern Physics B* (in preparation), (2004)
- 11 T G Leighton, S D Meers and P R White, A nonlinear time-dependent inversion to obtain bubble populations from acoustic propagation characteristics, *Proceedings of the Royal Society* (in press; published on Royal Society FirstCite Website May 2004)
- 12 <http://www.localauthoritypublishing.co.uk/councils/romsey/trail.html>
- 13 M G Kivelson, K K Khurana, C T Russell, M Volwerk, R J Walker and C Zimmer, Galileo magnetometer measurements: A stronger case for a subsurface ocean at Europa *Science* **289** (5483): 1340-1343 (2000)
- 14 M S Longuet-Higgins, Bubble noise spectra *JAoust Soc Am* **87**(2): 652-661 (1990)
- 15 T G Leighton, (editor), *Natural physical processes associated with sea surface sound*. University of Southampton (1997)

**T G Leighton** FIOA is Professor of Ultrasonics and Underwater Acoustics at the University of Southampton (ISVR). **P R White** is Senior Lecturer in Underwater Signal Processing at the University of Southampton (ISVR)